Controlled Close-Packing of Ferrimagnetic Nanoparticles: An Assessment of the Role of Interparticle Superexchange Versus Dipolar Interactions

ARTICLE *in* THE JOURNAL OF PHYSICAL CHEMISTRY C · APRIL 2013

Impact Factor: 4.77 · DOI: 10.1021/jp402444x

11 AUTHORS, INCLUDING:

Jose A. De Toro
University of Castilla-La Mancha
52 PUBLICATIONS **444** CITATIONS
SEE PROFILE

Florent Tournus
Claude Bernard University Lyon 1
83 PUBLICATIONS **1,313** CITATIONS
SEE PROFILE

A. Tamion
Claude Bernard University Lyon 1
48 PUBLICATIONS **526** CITATIONS
SEE PROFILE

Per Nordblad
Uppsala University
404 PUBLICATIONS **6,516** CITATIONS
SEE PROFILE

THE JOURNAL OF PHYSICAL CHEMISTRY C

Article

pubs.acs.org/JPCC

Controlled Close-Packing of Ferrimagnetic Nanoparticles: An Assessment of the Role of Interparticle Superexchange Versus Dipolar Interactions

Jose A. De Toro,*[,†] Peter S. Normile,[†] Su Seong Lee,[‡] Daniel Salazar,[†] Jian Liang Cheong,[‡] Pablo Muñiz,[†] Jose M. Riveiro,[†] Matthias Hillenkamp,[§] Florent Tournus,[§] Alexandre Tamion,[§] and Per Nordblad[∥]

[†]Instituto Regional de Investigación Científica Aplicada (IRICA) and Departamento de Física Aplicada, Universidad de Castilla-La Mancha, 13071 Ciudad Real, Spain

[‡]Institute of Bioengineering and Nanotechnology, 31 Biopolis Way, The Nanos, Singapore 138669, Singapore

[§]Institut Lumière Matière, UMR5306 University Lyon 1-CNRS, 69622 Villeurbanne, France

[∥]Department of Engineering Sciences, Uppsala University, Box 534, SE-751 21 Uppsala, Sweden

ABSTRACT: The fundamental question as to the relative importance of interparticle superexchange versus dipolar interaction between oxide magnetic particles in direct physical contact is addressed by examining the magnetic properties of a series of compacted samples comprising identical maghemite particles (8 nm in diameter) coated by nonmagnetic shells (oleic acid or silica) of varying thickness that control the distance between the magnetic cores and hence the packing density (particle volume fraction). A remarkably narrow maghemite particle size distribution is established by electron microscopy and small-angle X-ray scattering. The series includes a sample made up of bare particles in a random-close-packed configuration (therefore in direct contact) that exhibits ideal superspin-glass behavior with a relatively high freezing transition temperature. It is shown that interparticle superexchange interactions between the nanoparticles in this sample play a minor role compared to classical dipolar interactions in establishing the collective, superspin-glass state. This follows from the freezing temperature of the most concentrated samples in the series (those with 0 ≤ shell thickness < 3 nm), which are found to vary in direct proportionality with the volume fraction of the maghemite cores and therefore with the strength of dipolar interactions.

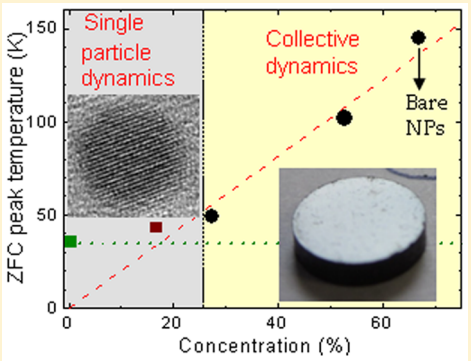

1. INTRODUCTION

Magnetic nanoparticles (NPs) receive much attention due to their application in a wide range of technologies,[1−4] many of which employ relatively dense ensembles of NPs, where interparticle interactions severely affect the magnetic properties of the resultant system.[2−4] However, there are still fundamental questions to be addressed regarding the role of certain types of interactions. Four kinds of interparticle coupling, as recently reviewed by Mørup et al.,[5] have been discussed in the literature (with different degrees of detail): classical dipolar or magnetostatic interactions (intensively studied),[6,7] RKKY-like coupling (studied in a few metallic granular films with a presence of solute magnetic atoms in the matrix),[8,9] direct exchange interactions (investigated in numerous percolated or quasi-percolated systems of ferromagnetic NPs),[7,10] and superexchange interactions (studied in a few instances involving antiferromagnetic oxide NPs).[5]

The last two types of interparticle coupling take place between NPs in direct physical contact. Direct exchange between metallic ferromagnetic (FM) NPs has been predicted and reported to greatly enhance the magnetization correlation length, yielding "correlated super-spin-glass"[11] or "superferromagnetic"[7] behavior (sometimes described using the random-anisotropy model[10,12]). However, there are only a few reports on the effects of superexchange between antiferromagnetic (AF) oxide particles, which mainly concluded a suppression of the superparamagnetic relaxation.[5] For the case of ferrimagnetic (FerriM) particles (the third type of NPs in terms of internal magnetic order, which are typically formed from Fe oxides), it remains unclear whether superexchange interactions may play a significant role in the magnetic order and dynamics of dense systems. At most, and in reference to a disordered packed system of maghemite NPs, it has been suggested that "the exchange interaction between surface atoms belonging to neighboring particles may be significant and this can further increase the (superspin-glass) ordering temperature".[13,14] Indeed, in such disordered particle systems, dipolar (randomly yielding parallel and antiparallel superspin alignments) and superexchange (expected to yield antiparallel alignments) interparticle interactions would combine to increase magnetic frustration and thus the temperature of the

Received: March 10, 2013
Revised: April 19, 2013
Published: April 22, 2013

   dx.doi.org/10.1021/jp402444x | J. Phys. Chem. C 2013, 117, 10213−10219

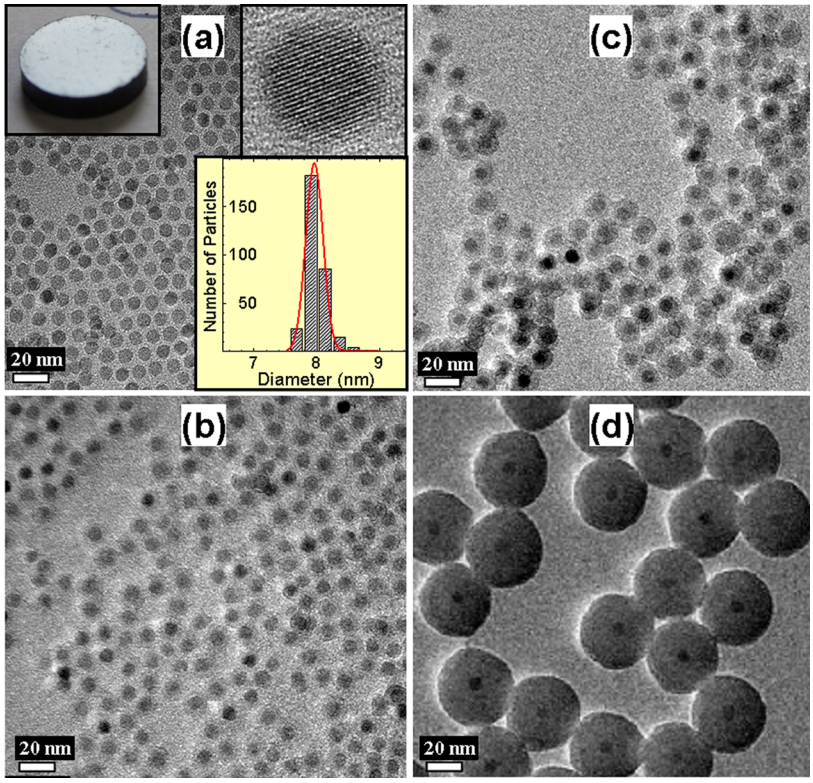

Figure 1. Transmission electron micrographs of bare maghemite nanoparticles (a) and the same particles coated with silica shells 2 nm (b), 3 nm (c), and 17 nm (d) thick. Insets in panel a, counterclockwise: particle size distribution and (undistinguishable) fits to log-normal and Gaussian functions; high-resolution TEM image of a nanoparticle; and photograph of the random-close-packed sample (RCP), a 6 mm diameter disc prepared with the bare particles.

transition (T_g) from a high temperature superparamagnetic regime to a collective superspin-glass state.

Of course, the use of the prefix super in "superexchange" refers to indirect exchange via a nonmagnetic ion (e.g., oxygen anion) positioned between two magnetic ions (e.g., iron cations), whereas other usage of this prefix (in "superspin" or "superparamagnetic") refers to the physics of particle macro-moments (each of the order of 10^2 to 10^4 μ_B). In the present article, we estimate the relative strength of superexchange with respect to dipolar interaction by comparing the transition temperature in a random-close-packed system of very uniform bare maghemite NPs (recently reported to exhibit ideal superspin-glass behavior,[15] i.e., mimicking that of conventional spin-glasses) with those measured in a number of packed ensembles of core−shell NPs with varying shell thickness (from ensemble to ensemble) and cores identical to the bare particles. This strategy to confidently achieve a narrow dispersion in interparticle (or, rather, intercore) distances has been successfully employed in previous studies.[16,17] We conclude that superexchange interactions between oxide ferrimagnetic NPs in direct physical contact play a minor role compared to dipolar interactions in establishing the glassy magnetic dynamics exhibited by this type of particle aggregate.

2. EXPERIMENTAL METHODS

2.1. Synthesis. Maghemite (γ-Fe_2O_3) nanoparticles were prepared according to the method reported by Hyeon et al.,[18] i.e., by thermal decomposition of iron pentacarbonyl followed by oxidation with trimethylamine *N*-oxide at high temperature. A temperature controller was used to accurately raise the solution temperature, which resulted in more uniform nanoparticles. The resulting solution was cooled down to room temperature, and acetone was added to yield a black precipitate. The precipitate was collected by a magnet and then washed with acetone and methanol. Both bare and coated nanoparticles (with either oleic acid or silica shells) were prepared from this precipitate. To prepare bare NPs, some particles were redispersed in *n*-hexane under sonication, precipitated by adding acetone, treated under sonication for one hour, and then recovered by precipitation. This process was repeated until the recovered nanoparticles were no longer dispersed in *n*-hexane under sonication. The collected nanoparticles were washed repeatedly with acetone and *n*-hexane under sonication and eventually dried under vacuum to give *bare* maghemite nanoparticles (as confirmed by the absence of any trace of oleic acid surfactant in Fourier transform infrared spectra). The rest of the NPs were left coated with oleic acid in cyclohexane after redispersing them in cyclohexane and then filtering the solution through a 0.2 μm PTFE filter.

For the synthesis of core−shell maghemite−silica particles (with shell thickness of 2, 3, and 17 nm), polyoxyethylene (5) nonylphenylether (5.0 g, Igepal CO-520, M_n = 441, Sigma-Aldrich) was dissolved in cyclohexane (60 mL), to which a solution of the above bare γ-Fe_2O_3 particles in cyclohexane (3.0 mL, 2.75 mg/mL in cyclohexane) was added. After stirring the resulting mixture, ammonium hydroxide (0.7 mL, 25% in water) was added to form a transparent brownish solution of reverse microemulsion. Next, tetraethyl orthosilicate (0.2 mL, TEOS) was added and the reaction was left to continue for 16 h at room temperature. For the thickest shell particles (with a shell thickness of 17 nm), ammonium hydroxide and TEOS were repeatedly added,and the shell size checked by TEM after

dx.doi.org/10.1021/jp402444x | J. Phys. Chem. C 2013, 117, 10213−10219

each addition and overnight stirring. Once the desired shell thickness was obtained, methanol (20 mL) was added into the reaction solution to break the microemulsion, leading to two separate phases. The core−shell particles were collected by centrifugation of the methanolic phase and thoroughly washed with cyclohexane [(5 × 5 mL) and methanol (5 × 5 mL)], then dried in vacuum.

After a mild homogenization using agate mortar and pebble, the different dry powders were uniaxially pressed under approximately 0.7 GPa to form five compact discs 6 mm in diameter and about 2 mm thick, hereafter referred to as (maghemite volume concentration in parentheses): Bare-RCP (67%), OA-coated (53%), S2-coated (27%), S3-coated (16%) and S17-coated (or reference) sample (0.4%), where OA and S denote oleic acid and silica, respectively. The acronym RCP stands for random-close-packed, a name that will be clearly justified in section 3. Only the NPs in the latter (reference) sample needed a mold release agent (zinc stearate) to form a uniform disc upon compression.

2.2. Structural and Magnetic Characterization Methods. The maghemite NPs crystalline structure and size dispersion were characterized using a Bruker D8 Advance X-ray diffractometer to measure wide- and small-angle scattering, respectively. The filling factor of the Bare-RCP disc was determined as the ratio of the disc density (measured using Archimedes' method) and the maghemite NP density extracted from X-ray diffraction. Transmission electron microscopy (TEM) was performed using an FEI Tecnai G2 F20 microscope operated at 200 kV using 400 Mesh Cu grids precoated with thin carbon film (Pacific Grid-Tech). The maghemite particle size distribution was obtained from a couple of randomly chosen areas from TEM images containing more than 300 nanoparticles. An MPMS Evercool SQUID magnetometer (Quantum Design) was employed for the magnetic characterization: magnetic response, thermal dependence of the magnetization after cooling in zero-field (ZFC) or in the field subsequently employed to register the data upon heating (FC), ZFC memory experiments where the cooling was stopped at T_S for three hours before resuming the cooling to the base temperature, and ac susceptibility as a function of temperature and frequency of the driving field.

3. STRUCTURAL CHARACTERIZATION

Figure 1 shows TEM micrographs of the bare and silica-coated maghemite particles. Panel a displays the bare NPs used to prepare the Bare-RCP disc (a photograph of this disc is shown in the left-hand inset). The NPs are highly crystalline, as evidenced by the HRTEM image (inset) of a single representative particle. The size (and shape) distribution is remarkably narrow (compared, e.g., with recently grown highly uniform iron oxide NPs[17,19,20]), with a log-normal fit (lower inset) of a 310 particle histogram (inset) yielding a median diameter d_{TEM} = 7.96 nm and a (log-normal) width parameter of σ_{TEM} = 0.017. Similarly, fitting to a Gaussian function gives an average diameter (±Gaussian width) of d_{TEM} = 7.96 (±0.14) nm. The silica-coated particles are likewise highly uniform.

The narrow NP size distribution of the maghemite NPs is confirmed from a macroscopic perspective by small-angle X-ray scattering (SAXS). Figure 2 shows SAXS data taken in transmission geometry on a specimen of the OA-coated NPs mounted on Kapton tape. The data, which have been fully background corrected, are indicative of a highly monodisperse distribution of spherical nanoparticles. This follows from the

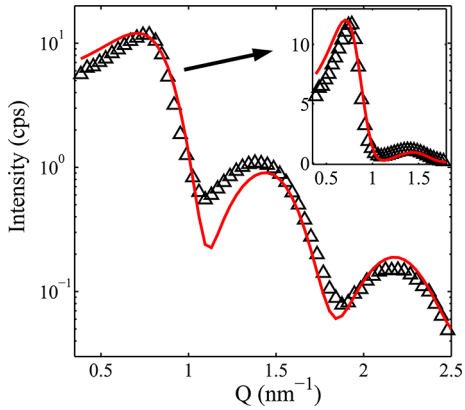

Figure 2. SAXS from OA-coated NPs. The fitting curve is described in the text. The inset shows the correlation and first oscillation peaks on a linear *y*-scale.

observation of the oscillations (at scattering vector $Q > 1$ nm^{-1}), which indicate a well-defined particle form factor, $P(Q)$, and hence particle diameter distribution, as well as from the sharp correlation peak (at $0.5 < Q < 1$ nm^{-1}), which points to a concomitantly well-defined structure factor, $S(Q)$, arising from the occurrence of NPs as particle aggregates in the studied (loose powder) specimen. The fitting curve is based on the product of these factors convoluted with the instrument resolution, $R(Q)$, i.e., intensity$(Q) \propto R(Q) \otimes [P(Q)S(Q)]$, where $P(Q)$ is the square of the Fourier transform (FT) of a solid sphere weighted by a very narrow Gaussian distribution of particle diameters, consistent with that obtained from TEM analysis. The $S(Q)$ follows from the FT of the pair distribution function of a random packing of hard solid spheres (here, the NP aggregates). The analytical form of $S(Q)$ can be found, for example, in ref 21. In the present fit, this function has been weighted by a Gaussian distribution in the packing density (particle volume fraction) parameter, yielding an average value of 0.41 with a Gaussian sigma width of 0.07, reasonable values for a loose powder specimen.[22]

Figure 3 shows wide-angle X-ray scattering (WAXS) data after background correcting and normalizing the different scans such that the strongest reflection, the (311), appears with the same peak intensity. From top to bottom, the scans are from (i) the Bare-RCP disc sample measured in Bragg−Brentano (BB) geometry, (ii) a specimen of OA-coated NPs supported on a glass slide and measured in BB geometry, and (iii) a quantity of the bare NPs mounted on Kapton tape and measured in transmission geometry. The respective values of lattice parameter determined from the fits (profile matching) to these scans are 8.341(4), 8.3450(15), and 8.3442(8) Å, which average at 8.344(1) Å, around 0.2% larger than the lattice parameter of bulk γ-Fe_2O_3 (8.33 Å), and point to a very slightly lower mass density in the nanocrystalline material as compared to the bulk; namely, 0.6% lower.

The density of the Bare-RCP disc was measured using Archimedes' method to be 3.28(2) g/cm^3, corresponding to a filling factor of 67% [ratio of the disc density and the particle density as derived from the lattice parameter from X-ray diffraction], a value only slightly above that corresponding to a random-close-packed (RCP) configuration.[23] This justifies our labeling of this sample as Bare-RCP.

dx.doi.org/10.1021/jp402444x | J. Phys. Chem. C 2013, 117, 10213−10219

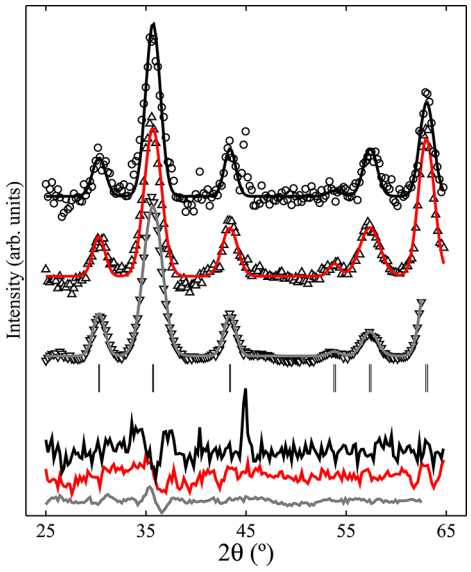

Figure 3. WAXS from three specimens from the same batch of NPs, fitted in order to determine the cubic (γ-Fe_2O_3) lattice parameter. Difference curves (data−fit) and reflection positions (black bars) are also shown. The bottom scan is cutoff at 62.7° owing to 2θ limitations in the transmission geometry.

4. MAGNETIC CHARACTERIZATION AND DISCUSSION

In the Bare-RCP disc, the maghemite concentration is equivalent to the above filling factor (67%). Thus, the saturation magnetization of the maghemite NPs can be accurately determined directly from a hysteresis loop (not shown). A value of M_S = 225 kA/m is obtained, which lies well within the wide range of values reported for maghemite (this parameter is quite sensitive to the actual distribution of cationic vacancies in the lattice[24,25]). This value has been used to unequivocally estimate the maghemite concentration in the other discs (given their saturation magnetic moments and sample volumes). These concentration values (see section 2.1) are similar to those expected from the shell thickness observed by TEM. The oleic acid in the OA-coated sample reduces the maghemite concentration from 67% (for bare particles) to 53%, effectively providing nonmagnetic shells thinner (upon compression) than those in the S2-coated sample.

The reference sample is magnetically diluted enough (0.4%) to allow for a reliable determination of single-particle parameters. The NP magnetic size distribution and the effective uniaxial anisotropy constant K were determined in this sample by simultaneously fitting the room temperature magnetic response, low field FC and ZFC magnetization curves, and the thermal dependence of ac susceptibility measured at different frequencies (Figure 4). This recently developed multiple-fit procedure, described in depth in refs 26 and 27, yields a median magnetic diameter of d_{MAG} = 7.9 nm (i.e., a particle superspin of $\mu \approx 6400\ \mu_B$), in excellent agreement with d_{TEM}, $K = 3.0 \times 10^4$ J/m^3 (a value similar to those previously found in maghemite NPs[13]), and a small log-normal polydispersity diameter index of σ_d = 0.16 (small compared, e.g., with the uniform NPs of Parker et al.[28]). Nonetheless, this magnetic dispersion is, as expected, significantly larger than that obtained above from TEM. The discrepancy can be understood as stemming from distributions of NP saturation moments and effective anisotropy, as well as from the higher sensitivity to the particle diameter of magnetometry ($\sim d^3$) compared with TEM ($\sim d$).[25]

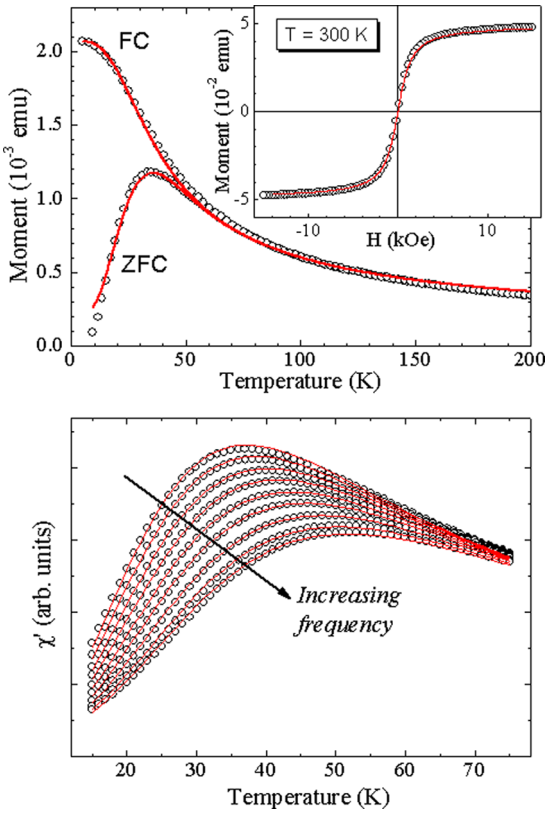

Figure 4. Simultaneous fit (red lines) of the thermal dependence of dc (upper panel) and ac (lower panel) magnetization of the S17-coated (reference) sample. Upper panel: field-cooled (FC) and zero-field-cooled (ZFC) magnetization curves, measured in a field of H = 5 Oe, and room temperature magnetic response (inset). Lower panel: real component of the ac susceptibility measured at frequencies of the driving field (with amplitude H_{ac} = 2 Oe) logarithmically scanning the available range (0.1−600 Hz).

Figure 5 compares the FC and ZFC curves measured in low field (H = 5 Oe) in the five discs. All the ZFC curves present a clear maximum at T_{peak}, which increases with the maghemite core concentration from 36 K in S17-coated to 145 K in Bare-

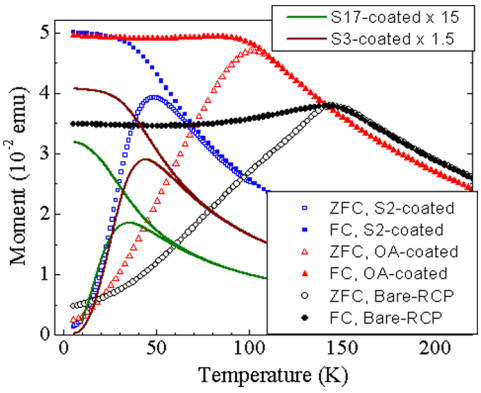

Figure 5. Field-cooled (FC) and zero-field- cooled (ZFC) magnetization curves measured in an applied field of H = 5 Oe in each of the five discs. The curves plotted as lines correspond to the more diluted samples (S3- and S17-coated), where no memory effect (see Figure 6) is observed.

dx.doi.org/10.1021/jp402444x | J. Phys. Chem. C 2013, 117, 10213−10219

RCP. The curves measured in the former sample exhibit all the features typical of isolated particle systems, including a strong FC-ZFC irreversibility between the two curves (with low temperature FC values far above the maximum magnetization in the ZFC curve) and a Curie–Weiss-like decay of the magnetization in the reversible region. The FC-ZFC irreversibility starts at temperatures slightly above T_{peak}, which is indicative, given the low measuring field, of a narrow moment distribution.[29] With decreasing shell thickness, the above features progressively change toward those, typically spin-glass-like, exhibited by the most concentrated sample (Bare-RCP), where the FC curve flattens out below T_{peak} and the FC-ZFC irreversibility begins very close to the ZFC maximum. These qualitative features, together with the increase in T_{peak} (to be analyzed in more detail below), reflect the increasingly strong interactions between the maghemite cores upon reducing the nonmagnetic shell thickness.

The three most concentrated samples (Bare-RCP and OA- and S2-coated) qualitatively differ from the two more diluted samples in the series (S3- and S17-coated) in that they exhibit the so-called "ZFC memory effect" as shown in Figure 6, which

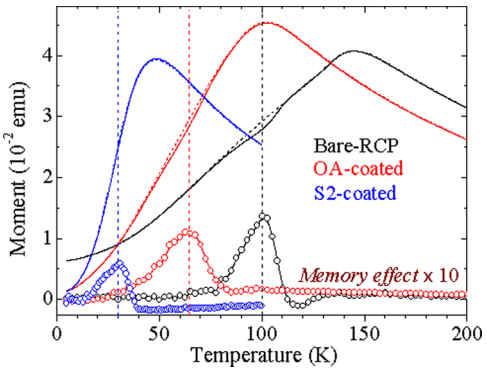

Figure 6. Memory effect (symbols and guides to the eye) measured in each of the three most concentrated samples as the difference between a standard ZFC curve (dotted line curve barely distinguishable from the solid line curve of the same color) and a ZFC curve (solid line) measured upon heating after stopping for 3 h during the cooling stage at the temperatures indicated by the vertical dashed lines.

reflects the characteristic chaotic dynamics of the spin-glass-like state.[30,31] When the system is zero-field cooled, a stop (for 3 h) performed at some temperature below the freezing temperature ($T_f \approx T_{peak}$), in this case $T_S \approx (2/3)T_f$, during cooling produces a dip when the magnetization is subsequently recorded upon heating from base temperature. The memory curve coincides with the reference curve at low temperatures (i.e., the system rejuvenates), and it merges with the reference curve at temperatures above the stop temperature. The memory effect, better observed in the rescaled difference plots also shown in Figure 6, weakens and broadens (in a relative T/T_{peak} scale) with increasing separation (therefore reducing interactions) between the maghemite cores. No memory effect could be detected above the measurement noise in the S3-coated sample. A multiple-stop memory experiment performed in the Bare-RCP sample is discussed with respect to results in other superspin-glasses in ref 15.

Since the bare particles in the Bare-RCP system are in direct physical contact, superexchange interactions between them (expected to yield antiparallel alignment of the macromoments) could be significant and contribute to frustration, thus increasing the SSG order temperature.[13] This possibility is explored in Figure 7 through the comparison of the ZFC peak

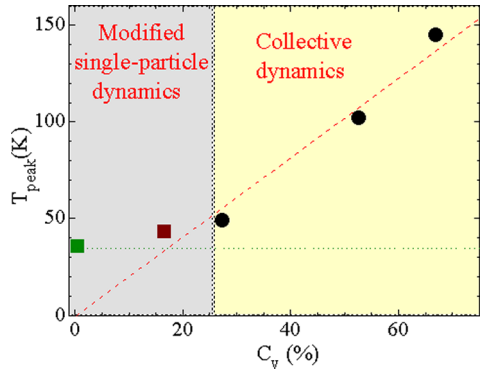

Figure 7. ZFC peak temperatures of all the samples in the series plotted as a function of maghemite core concentration. The dashed red line is a linear fit with zero-intercept of the higher concentration data points (black circles). The dotted horizontal green line marks the blocking temperature of the reference sample (isolated cores).

temperature (T_{peak}) in our series of differently concentrated samples comprising identical maghemite cores. The concentration dependence of T_{peak} reproduces the main features of the schematic phase-diagram proposed by Mørup for disordered dipolarly interacting particle systems:[32] a low concentration regime with a moderate variation of what can still be described as a blocking temperature (modified single-particle dynamics) followed by a steeper sloped linear dependence of a cooperative (freezing) transition essentially determined by the strength of interparticle interactions. Within this picture, the S2-coated sample, with its weak memory effect, seems to be close to the crossover between the two regimes. The freezing transition in the SSG systems (black circles) is closely proportional to the maghemite particle concentration (the red line is a linear fit with zero-intercept), i.e., to the strength of the dipolar interactions (in turn linearly dependent on the particle concentration and the here invariant average particle macromoment[33]). The relatively high[17,34] ratio (~4.0) between the freezing temperature in the Bare-RCP superspin-glass and the blocking temperature of the individual NPs (as measured in the magnetically diluted S17-coated disc) is thus concluded to largely be explained by the strong random dipolar interaction and not due to the contribution from additional superexchange interactions. In short, the Bare-RCP sample is an essentially dipolar superspin-glass.

As for the modified single-particle regime in Figure 7, it must be noted that Mørup et al.'s theoretical prediction (and Mössbauer observation) was a reduction in T_{peak}, rather than an increase, upon the introduction of weak interactions. However, the opposite behavior, as found here, has been reported in several magnetometry studies.[35−37] We plan to prepare packed samples of NPs with thick silica shells in an attempt to elucidate whether those two differing behaviors can be reconciled by ascribing them to different regimes of weak/very weak dipolar interactions.

5. CONCLUSIONS

In summary, despite the close contact of the maghemite particles in the Bare-RCP sample enabling superexchange interactions, the system's freezing temperature hardly deviates from the value expected exclusively from dipolar interactions.

dx.doi.org/10.1021/jp402444x | J. Phys. Chem. C 2013, 117, 10213−10219

This assertion has been made possible by the comparison between differently concentrated systems of identical maghemite particles. Indeed, a dominant role of dipolar interactions may be expected from the much larger moment of the γ-Fe_2O_3 ferrimagnetic NPs in our random-close-packed system compared with that of AF particles where superexchange effects have been observed.[5] More generally, this result establishes that superexchange interactions play a minor role in dense systems of ferrimagnetic oxide particles. Such a fundamental finding simplifies the modeling involved in various applications based on magnetic oxide particle aggregates, e.g., in data storage, high frequency devices, or even in cancer therapy specifically relying on interparticle interactions.[2] It also encourages the experimental search for dipolar superferromagnets and -antiferromagnets in ordered lattices (as predicted in Luttinger and Tisza's seminal work[38]) of oxide NPs without the need of using any coatings.

AUTHOR INFORMATION

Corresponding Author

* (J.A.D.T) E-mail: joseangel.toro@uclm.es.

Notes

The authors declare no competing financial interest.

ACKNOWLEDGMENTS

We acknowledge financial support from the Spanish CICYT [MAT2011-26207], the Institute of Bioengineering and Nanotechnology (Biomedical Research Council, Agency for Science, Technology and Research, Singapore), the Swedish Research Council, and the Centre de Magnétométrie de Lyon (CML).

REFERENCES

(1) Reiss, G.; Hütten, A. Magnetic Nanoparticles: Applications Beyond Data Storage. *Nat. Mater.* **2005**, *4*, 725−726.

(2) Dobson, J. Death by Magnetism. *Nat. Mater.* **2012**, *11*, 1006−1008.

(3) Sun, S.; Murray, C. B.; Weller, D.; Folks, L.; Moser, A. Monodisperse FePt Nanoparticles and Ferromagnetic FePt Nanocrystal Superlattices. *Science* **2000**, *287*, 1989−1992.

(4) Rebolledo, A. F.; Fuertes, A. B.; Gonzalez-Carreño, T.; Sevilla, M.; Valdes-Solís, T.; Tartaj, P. Signatures of Clustering in Superparamagnetic Colloidal Nanocomposites of an Inorganic and Hybrid Nature. *Small* **2008**, *4*, 254−261.

(5) Mørup, S.; Hansen, M. F.; Frandsen, C. Magnetic Interactions Between Nanoparticles. *Beilstein J. Nanotechnol.* **2010**, *1*, 182−190.

(6) Jönsson, P. E. Superparamagnetism and Spin Glass Dynamics of Interacting Magnetic Nanoparticle Systems. *Adv. Chem. Phys.* **2004**, *128*, 191−248.

(7) Bedanta, S.; Kleemann, W. Supermagnetism. *J. Phys. D: Appl. Phys.* **2009**, *42*, 013001.

(8) De Toro, J. A.; Andrés, J. P.; González, J. A.; Goff, J. P.; Barbero, A. J.; Riveiro, J. M. Improved Giant Magnetoresistance in Nanogranular Co/Ag: The Role of Interparticle RKKY Interactions. *Phys. Rev. B* **2004**, *70*, 224412.

(9) Du, J.; Zhang, B.; Zheng, R. K.; Zhang, X. X. Memory Effect and Spin-Glass-like Behavior in Co−Ag Granular Films. *Phys. Rev. B* **2007**, *75*, 014415.

(10) Alonso, J.; Fdez-Gubieda, M.; Barandiarán, J.; Svalov, A.; Fernández Barquín, L.; Alba Venero, D.; Orue, I. Crossover from Superspin Glass to Superferromagnet in Fe_xAg_{100-x} Nanostructured Thin Films ($20 \leq x \leq 50$). *Phys. Rev. B* **2010**, *82*, 054406.

(11) Binns, C.; Maher, M. J.; Pankhurst, Q. A.; Kechrakos, D.; Trohidou, K. N. Magnetic Behaviour of Nanostructured Films Assembled from Pre-Formed Fe Clusters Embedded in Ag. *Phys. Rev. B* **2002**, *66*, 184413.

(12) Nunes, W.; Socolovsky, L.; Denardin, J.; Cebollada, F.; Brandl, A.; Knobel, M. Role of Magnetic Interparticle Coupling on the Field Dependence of the Superparamagnetic Relaxation Time. *Phys. Rev. B* **2005**, *72*, 212413.

(13) Mørup, S.; Bodker, F.; Hendriksen, P. V.; Linderoth, S. Spin-Glass-Like Ordering of the Magnetic Moments of Interacting Nanosized Maghemite Particles. *Phys. Rev. B* **1995**, *52*, 287.

(14) Mørup, S.; Madsen, M. B.; Franck, J.; Koch, C. J. W. A New Interpretation of Mössbauer Spectra of Microcrystalline Goethite: "Super-Ferromagnetism" or "Super-Spin-Glass" Behaviour? *J. Magn. Magn. Mater.* **1983**, *40*, 163−174.

(15) De Toro, J. A.; Lee, S. S.; Salazar, D.; Cheong, J. L.; Normile, P. S.; Muñiz, P.; Riveiro, J. M.; Hillenkamp, M.; Tournus, F.; Tamion, A.; et al. A Nanoparticle Replica of the Spin-Glass State. *Appl. Phys. Lett.* **2013**, DOI: http://dx.doi.org/10.1063/1.4804187.

(16) Papaefthymiou, G. C.; Devlin, E.; Simopoulos, A.; Yi, D.; Riduan, S.; Lee, S. S.; Ying, J. Interparticle Interactions in Magnetic Core/Shell Nanoarchitectures. *Phys. Rev. B* **2009**, *80*, 024406.

(17) Hiroi, K.; Komatsu, K.; Sato, T. Superspin Glass Originating from Dipolar Interaction with Controlled Interparticle Distance Among γ-Fe_2O_3 Nanoparticles with Silica Shells. *Phys. Rev. B* **2011**, *83*, 224423.

(18) Hyeon, T.; Lee, S. S.; Park, J.; Chung, Y.; Na, H. B. Synthesis of Highly Crystalline and Monodisperse Maghemite Nanocrystallites Without a Size-Selection Process. *J. Am. Chem. Soc.* **2001**, *123*, 12798−12801.

(19) Kasyutich, O.; Desautels, R. D.; Southern, B. W.; van Lierop, J. Novel Aspects of Magnetic Interactions in a Macroscopic 3D Nanoparticle-Based Crystal. *Phys. Rev. Lett.* **2010**, *104*, 127205.

(20) Vogt, C.; Toprak, M. S.; Muhammed, M.; Laurent, S.; Bridot, J.-L.; Müller, R. N. High Quality and Tuneable Silica Shell−Magnetic Core Nanoparticles. *J. Nanopart. Res.* **2009**, *12*, 1137−1147.

(21) Ashcroft, N. W.; Lekner, J. Structure and Resistivity of Liquid Metals. *Phys. Rev.* **1966**, *145*, 83−90.

(22) Wouterse, A.; Philipse, A. P. Geometrical Cluster Ensemble Analysis of Random Sphere Packings. *J. Chem. Phys.* **2006**, *125*, 194709.

(23) Song, C.; Wang, P.; Makse, H. A. A Phase Diagram for Jammed Matter. *Nature* **2008**, *453*, 629−632.

(24) Li, D.; Teoh, W. Y.; Woodward, R. C.; Cashion, J. D.; Selomulya, C.; Amal, R. Evolution of Morphology and Magnetic Properties in Silica/Maghemite Nanocomposites. *J. Phys. Chem. C* **2009**, *113*, 12040−12047.

(25) Yusuf, S. M.; De Teresa, J. M.; Mukadam, M. D.; Kohlbrecher, J.; Ibarra, M. R.; Arbiol, J.; Sharma, P.; Kulshreshtha, S. K. Experimental Study of the Structural and Magnetic Properties of γ-Fe_2O_3 Nanoparticles. *Phys. Rev. B* **2006**, *74*, 224428.

(26) Tamion, A.; Hillenkamp, M.; Tournus, F.; Bonet, E.; Dupuis, V. Accurate Determination of the Magnetic Anisotropy in Cluster-Assembled Nanostructures. *Appl. Phys. Lett.* **2009**, *95*, 062503.

(27) Hillion, A.; Pauly, M.; Tamion, A.; Tournus, F.; Hillenkamp, M.; Pichon, B. P.; Begin-Colin, S.; Dupuis, V. Combined Fitting of Alternative and Direct Susceptibility Curves of Assembled Nanostructures. *J. Appl. Phys.* **2012**, *112*, 123902.

(28) Parker, D.; Dupuis, V.; Ladieu, F.; Bouchaud, J.; Dubois, E.; Perzynski, R.; Vincent, E. Spin-Glass Behavior in an Interacting γ-Fe_2O_3 Nanoparticle System. *Phys. Rev. B* **2008**, *77*, 104428.

(29) Hansen, M. F. Estimation of Blocking Temperatures from ZFC/FC Curves. *J. Magn. Magn. Mater.* **1999**, *203*, 214−216.

(30) Mathieu, R.; Jönsson, P. E.; Nam, D.; Nordblad, P. Memory and Superposition in a Spin Glass. *Phys. Rev. B* **2001**, *63*, 092401.

(31) Sahoo, S.; Petracic, O.; Kleemann, W.; Nordblad, P.; Cardoso, S.; Freitas, P. P. Aging and Memory in a Superspin Glass. *Phys. Rev. B* **2003**, *67*, 214422.

(32) Mørup, S. Superparamagnetism and Spin Glass Ordering in Magnetic Nanocomposites. *Europhys. Lett.* **1994**, *28*, 671−676.

(33) Hansen, M. F.; Mørup, S. Models for the Dynamics of Interacting Nanoparticles. *J. Magn. Magn. Mater.* **1998**, *184*, L262−274.
(34) Hansen, M. F.; Jönsson, P. E.; Nordblad, P.; Svedlindh, P. Critical Dynamics of an Interacting Magnetic Nanoparticle System. *J. Phys.: Condens. Matter* **2002**, *14*, 4901−4914.
(35) Dormann, J. L.; Bessais, L.; Fiorani, D. A Dynamic Study of Small Interacting Particles: Superparamagnetic Model and Spin-Glass Laws. *J. Phys. C: Solid State Phys.* **1988**, *21*, 2015−2034.
(36) Dormann, J. L.; Fiorani, D.; Tronc, E. On the Models for Interparticle Interactions in Nanoparticle Assemblies: Comparison with Experimental Results. *J. Magn. Magn. Mater.* **1999**, *202*, 251−267.
(37) De Toro, J. A.; González, J.; Normile, P. S.; Muñiz, P.; Andrés, J.; López Antón, R.; Canales-Vázquez, J.; Riveiro, J. Energy Barrier Enhancement by Weak Magnetic Interactions in Co/Nb Granular Films Assembled by Inert Gas Condensation. *Phys. Rev. B* **2012**, *85*, 054429.
(38) Luttinger, J. M.; Tisza, L. Theory of Dipole Interaction in Crystals. *Phys. Rev.* **1946**, *70*, 954−964.